JOURNAL OF PROPULSION AND POWER
Vol. 16, No. 3, May–June 2000

Line-of-Sight Variations of Temperature and Species in Solid Propellant Flames

Carl F. Mallery Jr.* and Stefan T. Thynell†
Pennsylvania State University, University Park, Pennsylvania 16802

The purpose of this work is to deduce line-of-sight variations of temperature and species concentrations in high-pressure, solid-propellant flames by using spectral transmittances acquired by Fourier transform infrared spectrometry. To deduce these variations, an inverse technique was developed. For its validation, temperature and mole-fraction profiles within nitramine-composite propellant flames at low pressures were compared with similar measurements made by using fine-wire thermocouples and a microprobe mass spectrometer. Subsequently, it was applied to spectral transmittance data acquired for a high-pressure, self-sustained solid-propellant flame. Several conclusions were made. First, at about 3–4 mm above the surface, one must account for line-of-sight variations. Second, the deduced centerline temperatures were within 50 K of those measured using fine-wire thermocouples. Finally, the deduced centerline concentrations of CO and NO established a dark-zone behavior, which is expected of nitramine-composite propellant flames. However, to deduce the line-of-sight variation of other infrared-active species, further improvements in the database of the spectral absorption coefficients must be made.

Nomenclature

B	= signal intensity in wavenumber domain
B_0	= rotational constant
c	= speed of light
$\boldsymbol{D}$	= Hessian matrix
E'	= rotational energy of lower state
F	= spectral transmittance
f	= instrument response function
h	= Planck's constant
I	= intensity
k	= Boltzmann's constant
L	= path length
M_P, M_T	= upper limit of expansion in Eq. (5)
N_d	= number of data points in measurement
N_r	= number of rovibrational transitions
N_s	= number of species
P_i	= partial pressure of ith species
$P_{i,m}$	= coefficients for partial-pressure profile of ith species
R_f	= radius of flame
r	= radial position within Fourier transform infrared (FTIR)/flame interaction region, $r = \sqrt{(R_f^2 - x^2)}$
S	= line intensity
T	= temperature
T_m	= coefficients for temperature profile
$X_n(x)$	= row vector of species mole fractions
x	= distance along direction of beam propagation within the FTIR/flame interaction region
y	= distance along the width of FTIR beam within the FTIR/flame interaction region
$\hat{\boldsymbol{Z}}$	= vector of M estimated parameters
α	= absorption coefficient
β	= integrated absorption coefficient
$\Delta_{\max}$	= maximum retardation of moving mirror
δ	= purge gas mixing thickness
ζ	= r/R_f
ν	= wavenumber
ν_0	= fundamental vibrational wavenumber for CO
σ	= standard deviation
χ^2	= least-squares norm
ω	= Gaussian distribution function

Subscripts

b	= background
c	= core flame condition
i	= ith species
j	= jth rovibrational transition
meas	= measured quantity
noise	= quantity affected by noise
o	= rovibrational line center
p	= purge gas quantity
r	= reference state
s	= sample quantity
true	= true quantity
δ	= purge gas mixing region quantity

Superscripts

$\hat{}$	= modeled quantity
$\tilde{}$	= measured quantity

I. Introduction

RECENT efforts focused on one-dimensional ignition and steady deflagration models of solid propellants[1–3] with detailed finite-rate chemical kinetics[3,4] have significantly increased the demand for accurate data on the variation of temperature and species concentrations in the direction of flow of products. Experimental data acquired at and along the centerline within the flame should be particularly useful in validating these complex models.[5] Many measurements using strand burners have been reported using line-of-sight (LOS) techniques, such as UV-visible,[6,7] multichannel mid-infrared,[8] and Fourier transform infrared (FTIR)[9] spectroscopy. Although temperature and species concentrations can vary along the LOS within the flame, it appears that many investigators have not accounted for this effect in their data-reduction analysis. In essence, their results represent a weighted average of temperature and species concentrations over the measurement's path length. It is evident that mathematical methods should be developed that provide an insight into the variations of temperature and species concentration along the LOS.

In past research with LOS instruments, investigators employed multiple paths through the flame for radial temperature and species

Received 20 November 1998; revision received 3 May 1999; accepted for publication 6 May 1999.

*Graduate Research Assistant and University Research Initiative Fellow; currently Project Engineer, Ensign Bickford Company, 660 Hopmeadow Street, P.O. Box 483, Simsbury, CT 06070.

†Professor, Department of Mechanical and Nuclear Engineering. Senior Member AIAA.

concentration profiling along with Abel's inversion technique.[10] Premixed[11] and diffusion[12] flames are well suited to inversion techniques because the flames are stable and fixed in space to allow probing at different radial positions. However, the use of multiple paths in solid propellants is quite challenging in view of the required high pressures (which optically limits the flame width), relatively high burning rates, and a moving burning surface (short measurement times, generally 30 s or less). Therefore, new data-reduction methods must be developed to account for spatial variations in temperature and species concentrations within solid-propellant flames.

The objective of this work is to describe the approach and results obtained from profiling high-pressure propellant flames using FTIR transmission spectroscopy and a single LOS. In previous works, it has been shown that radial variations of temperature and species concentrations must be considered in high-pressure propellant flames.[9] To account for such variations, a theoretical approach was developed and applied to examining synthetic flames.[13] It is now extended to actual flames, in which the effects of noise are assessed.

II. Theory and Data Reduction

Let us consider that the modulated beam of an FTIR spectrometer propagates through a solid-propellant flame as depicted in Fig. 1. The flame is assumed to be axisymmetric so that temperature and species partial pressures vary only radially and vertically. Within the modulated beam, however, vertical variations of temperature and species concentration are assumed to be negligible. The beam travels across the entire propellant flame, perpendicular to the flow direction of hot gases, with the transmitted component detected by the spectrometer. In developing a model of the spectral transmittance, the interaction of the modulated beam with combustion gases, along with effects arising from the instrument itself, must be considered.

A. Model of Spectral Transmittance

In modeling the spectral transmittance acquired by an FTIR spectrometer operating at a low spectral resolution, the instrumental effects must be considered to deduce temperature and species concentrations correctly.[14] By assuming that spectral lines cannot be resolved, a convolution of the true transmittance with the instrument line shape should reproduce the measured spectral transmittance $F(\nu)$. Such a convolution may be expressed by

$$F(\nu) = \int_{-\infty}^{\infty} F_{\text{true}}(\nu')\, f(\nu - \nu')\, \mathrm{d}\nu' \tag{1}$$

For triangular apodization, the instrument line shape is[14]

$$f(\nu - \nu') = \frac{\Delta_{\max} \sin^2[\pi \Delta_{\max}(\nu - \nu')]}{[\pi \Delta_{\max}(\nu - \nu')]^2} \tag{2}$$

For molecular gases, such as those that appear in most solid-propellant flames, scattering is negligible compared to absorption. If small absorbing particles are present, such as soot, they possess broadband absorption characteristics, which can be removed in the analysis. The true spectral transmittance can therefore be written as

$$F_{\text{true}}(\nu) = \frac{1}{R_f} \int_0^{R_f} \exp\left[-2 \int_0^{\sqrt{R_f^2 - y^2}} \sum_{i=1}^{N_s} \sum_{j=1}^{N_r} \alpha_{i,j}[\nu, T(r), X_n(r)] P_i(r)\, \mathrm{d}x \right] \mathrm{d}y \tag{3}$$

The absorption coefficient $\alpha_{i,j}$ is evaluated using the HITRAN database.[15] A detailed discussion on the evaluation of line-broadening effects are available[13] and not repeated here. Nitrogen is the only infrared (IR)-inactive gas considered; its mole fraction is evaluated from

$$X_{N_2} = 1 - \sum_{i=1}^{N_s} X_i \tag{4}$$

However, hydrogen could also be an important product, but it is also IR-inactive at the pressures of interest. The use of Eq. (4) yields the mole fractions of both nitrogen and hydrogen. In addition, the integrals in Eqs. (1) and (3) are evaluated numerically using Gauss–Legendre quadratures,[16] and their accuracy has been assessed.[13]

B. Inverse Problem

The use of Eq. (3) in an inverse model allows a determination of radial temperature and partial-pressure profiles from spectral transmittance data. In this work, the temperature and partial pressures are assumed to vary according to a power series containing only even-ordered terms. The functional forms of the temperature and partial-pressure profiles are, respectively, given by

$$T(\zeta) = \sum_{m=0}^{M_T} T_m \zeta^{2m} \qquad \text{and} \qquad P_i(\zeta) = \sum_{m=0}^{M_P} P_{i,m} \zeta^{2m} \tag{5}$$

The maximum temperature is located along the centerline within the propellant flame because it burns in a cool, inert atmosphere. The species profiles are, in most cases, monotonically decreasing functions from the centerline to the edge of the flame. A large number of spectral transmittances are employed in the inverse problem. The inverse problem is solved using a nonlinear least-squares method that seeks to minimize the quantity[16,17]

$$\chi^2 = \sum_{n=1}^{N_d} \left[\frac{\tilde{F}_n - \hat{F}_n(\hat{\boldsymbol{Z}})}{\sigma_n} \right]^2 \tag{6}$$

The vector $\hat{\boldsymbol{Z}}$ contains M estimated coefficients in Eqs. (5). Convergence of the iterative procedure is established when the change in χ^2 from one iteration to the next is $< 10^{-4}$. Confidence bounds for the estimated parameters can be calculated using the Hessian matrix. The standard deviations of the deduced parameters are given by[18]

$$[\sigma(\hat{\boldsymbol{Z}})]^2 = \frac{\mathrm{diag}[\boldsymbol{D}^{-1}]}{\sigma_{\text{meas}}^2} \tag{7}$$

These standard deviations, obtained from the inverse model itself, provide an estimate of the accuracy of the deduced parameters.

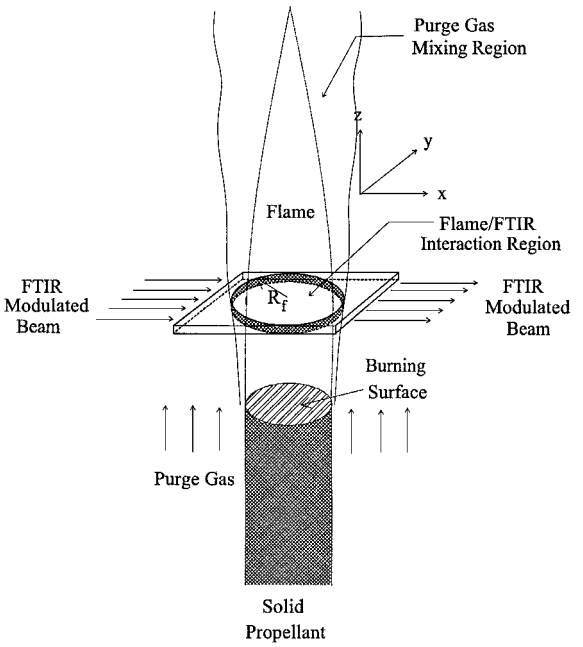

Fig. 1 Schematic diagram of the FTIR beam propagation through the solid-propellant flame.

III. Discussion of Results

To illustrate the approach of the inverse analysis, results from species profiling of a laser-assisted, low-pressure nitramine-composite propellant flame (XM39) are first compared with those obtained by using a microprobe mass spectrometer (MPMS). Second, the approach for dealing with LOS variations and selection of spectral range of the inverse technique are discussed. Finally, the results of centerline temperatures and species concentrations are shown. The spectrometer operates at a spectral resolution of 1.93 cm^{-1} with triangular apodization. It is equipped with a KBr beamsplitter and a mercury-cadmium-telluride detector.[9]

A. Validation of Algorithm

To provide a comparison with other diagnostic techniques,[19] results from a MPMS were utilized.[20] These comparisons were made on the nitramine-composite propellant XM39. The tests were conducted under CO_2 laser-assisted conditions at 1 atm because self-sustained combustion of the propellant in a nitrogen atmosphere cannot be achieved at this pressure. From heat flux calibrations, the propellant received a laser flux of 65 W/cm^2. Profiles of relative species mole fractions ($P_i / \Sigma_{i=1}^{N} P_i$) for NO, N_2O, CO_2, CO, and NO_2 ($N = 5$) deduced from the two measurement techniques are shown in Fig. 2. In this figure, only LOS average concentrations were deduced. It should be noted that the FTIR profiles were shifted 2 mm to the left (toward the burning surface). Such shifts were required because the combustion products expanded appreciably in the radial direction when no purge gas was utilized. With purge gas, the radial expansion was minimized; the net effect was a flame that positioned itself further from the surface compared to the case without using a purge gas. Relative mole-fraction profiles from the two techniques agree in both trends and magnitude for the five species considered.

The relative mole fractions of N_2O show the greatest deviation. This is consistent with calibration tests discussed elsewhere,[20,21] in which N_2O concentrations deduced by FTIR spectroscopy and the actual concentration in the calibration gas differed by about 9%. The same gases were used to calibrate the MPMS. The FTIR-deduced relative mole fractions have more scatter than the MPMS data. This is primarily because of the effects of the CO_2 laser, which produced small, pulsed overtone lines in the mid-IR that increased the noise level. However, purge gas mixing also caused variations in temperature and species along the LOS. Mole fractions of CH_2O and HCN were also deduced by both measurement techniques, but are not compared because of the poor fit between the measured and modeled transmittances of these molecules. The poor fit to the ν_1, ν_4, and $2\nu_3$ bands of CH_2O in the 2800 cm^{-1} region (only spectral region in which HITRAN has radiative properties for CH_2O) resulted from strong interference with the $\nu_1 + \nu_3$ overtone band of NO_2 and the high noise level. Inaccuracies in the HITRAN database and the high level of noise resulted in the poor fit to the HCN transmittances.

The agreement in magnitudes and trends of the mole-fraction profiles provides confidence in the ability of both measurement techniques. These measurements are needed to validate complex combustion models and to provide insight into the chemical kinetics. For instance, reactions of CH_2O and NO_2 to form CO, NO, and H_2O are believed to cause the main heat release in the primary reaction zone of nitramine-based propellants.[3,4] As shown in Fig. 2, a reduction in NO_2 accompanied an increase in CO and NO concentrations to support this reaction mechanism.

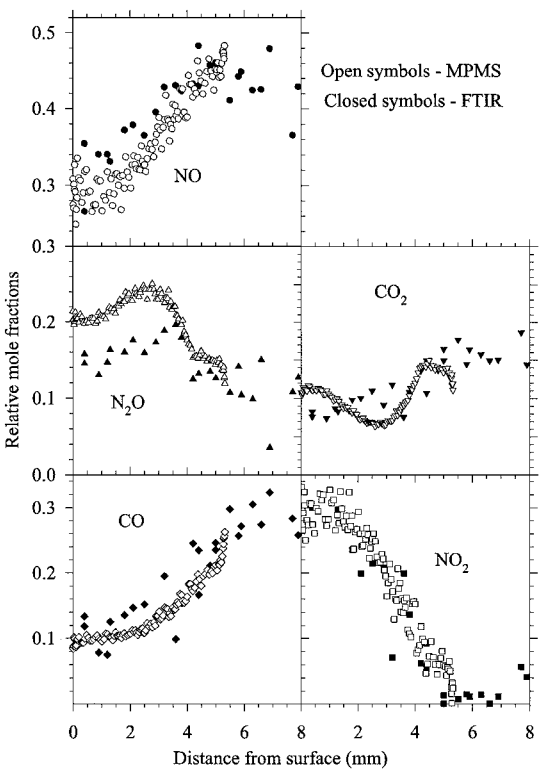

Fig. 2 Measured CO, CO_2, NO, N_2O, and NO_2 relative mole-fraction profiles during laser-assisted deflagration of XM39 at 1 atm and 65 W/cm^2 using FTIR spectroscopy and MPMS.

B. Selection of Spectral Regions

The influence of the mixing region, as illustrated in Fig. 1, on the spectral transmittance will be explored using an idealized one-dimensional flame. The temperature and partial pressure variations along the LOS for this idealized flame are shown in Fig. 3. Understanding the impact of the mixing region allows the optimal spectral range to be chosen for data reduction.

The impact of the mixing region on the transmittance data comes through Eq. (3), whose exponent is the spectral optical distance, and it will be explored using linearly varying temperature and partial-pressure profiles as shown in Fig. 3. This study will provide insight into the effects of the physical parameters, such as flame temperature, purge temperature, partial-pressure variations through the mixing region, and rovibrational transitions, on the spectral optical distance, which is given by

$$\beta = \left[\int_0^{L_c} + \int_{L_c}^{x = L_c + \delta} \right] \alpha[T(x)] P_i(x)\, \mathrm{d}x = \beta_c + \beta_\delta \tag{8}$$

For a diatomic molecule and profiles shown in Fig. 3, β_δ can be evaluated allowing the establishment of its functional relationship to the physical parameters of interest. The following expression for the optical distance ratio β_δ / β_c is found.

$$\frac{\beta_\delta}{\beta_c} = \frac{\delta}{L_c} \frac{k}{hc(T_c - T_p) P_{i,c}} \left(P_{i,c} - \frac{P_{i,c} - P_{i,p}}{T_c - T_p} T_c \right) \times \left(T_c^2 \Psi(T_c, E') - \frac{\alpha(T_p)}{\alpha(T_c)} T_p^2 \Psi(T_p, E') \right) + \frac{\delta}{L_c} \frac{P_{i,c} - P_{i,p}}{(T_c - T_p)^2} \frac{S(T_r) B_0 hc}{\alpha(T_c) P_{i,c} k} \Gamma(T_c, T_p) \tag{9}$$

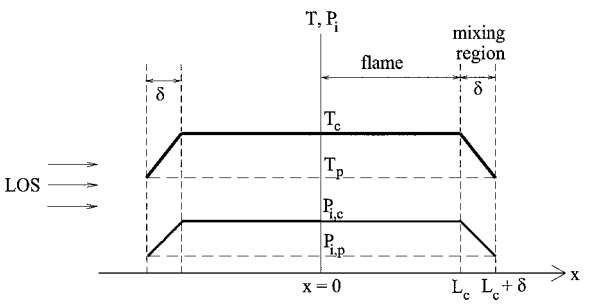

Fig. 3 Temperature and partial-pressure profiles of an idealized, one-dimensional flame used to ascertain the impact of a mixing region on the spectral optical distance.

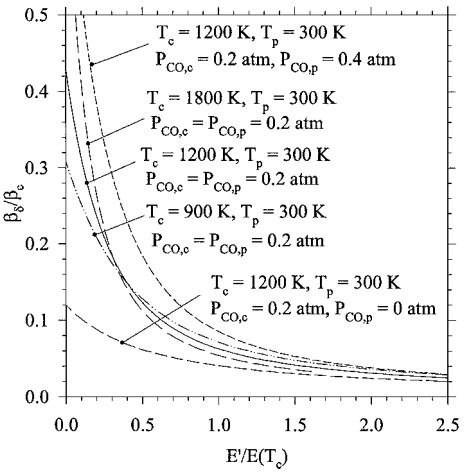

Fig. 4 Importance of spectral optical thickness of purge gas mixing region.

where

$$\Psi(T, E') = \frac{1}{\nu_0 + E'} + \frac{\nu_0}{E'(\nu_0 + E')[1 - \exp(-hc\nu_0/kT)]} \quad (10)$$

and

$$\Gamma(T_c, T_p) = -\int_{1/T_p}^{1/T_c} \{\exp(-hcE'u/k) - \exp[-hc(E' + \nu_0)u/k]\}u^{-1}\,du \quad (11)$$

The integral in Eq. (11) is evaluated numerically. The optical distance is linearly dependent on both the mixing-layer thickness and the variation in the partial pressure through the mixing layer. As discussed in Sec. II, the spectral transmittance has a nonlinear relationship with temperature that depends on the rovibrational transition. This relationship was exploited in the data-reduction algorithm to determine spatial variations in temperature and partial pressure.

The goal is to use Eqs. (9–11) to select the optimal spectral range for data reduction. The spectral dependence is not obvious from the equations, so the variation in β_δ/β_c with $E'/E(T_c)$ for several different flame temperatures ($T_p = 300$ K) is plotted in Fig. 4. A mixing region thickness of 0.5 mm (10% of the physical path length) along with radiative properties for the P branch of CO were used in the calculation of β_δ/β_c. For a diatomic molecule, E' is easily related to the wavenumber domain, whereas $E(T)$ is a function of the molecule and the flame temperature.[22] The rovibrational lower-state energy at which the absorption coefficient reaches a maximum with respect to temperature corresponds to $E(T)$. The spectral absorption coefficient corresponding to the rovibrational transition with $E' = E(T_c)$ is the most sensitive to the flame temperature T_c. From Fig. 4, the mixing region has a small impact on the optical distance ratio when $E' > E(T_c)$. However, the mixing region has a large impact on this ratio when the lower-state energy is much less than $E(T_c)$. The extent of the impact of the mixing region on the transmittance measurement will depend on the physical parameters (T_c, T_p, $P_{i,c}$, $P_{i,p}$, L_c) as well as the geometry of the measurement beam/flame interaction region.

The ability to deduce flame parameters when a mixing region exists will be explored using synthetically generated transmittance spectra. The synthetic spectra will also be used to select the spectral ranges for data reduction when probing an axisymmetric flame in which the LOS variations of temperature and species concentrations are large. In such a case, the algorithm should use a spectral region sensitive to a range of temperatures to determine the radial temperature and partial-pressure profiles. Finally, this section concludes with a brief discussion concerning the effect of interference from neighboring molecules on the determination of species and temperature distribution as well as on the proper selection of spectral regions for data reduction.

Table 1 Influence of the spectral range used for data reduction on temperature and CO partial-pressure predictions, with synthetic centerline temperature and partial pressure of 1300 K and 4 atm, respectively

	σ = 0.000		σ = 0.001		σ = 0.005	
Range, cm^{-1}	T, K	P_{CO}, atm	T, K	P_{CO}, atm	T, K	P_{CO}, atm
1910–1990	1269	3.610	1263	3.636	1240	3.738
1930–2010	1262	3.639	1260	3.649	1254	3.690
1950–2030	1254	3.660	1257	3.659	1268	3.654
1970–2050	1243	3.673	1245	3.675	1253	3.686
1990–2070	1219	3.657	1221	3.660	1228	3.670
2010–2090	1184	3.589	1182	3.584	1177	3.567
2030–2110	1140	3.449	1140	3.449	1139	3.447

Small Purge Gas Mixing Region

To demonstrate the application of $E(T)$ in the selection of spectral ranges, the data-reduction algorithm was executed assuming that the temperature and partial pressure of CO were uniform along the LOS. The synthetic spectrum, representing synthetically generated experimental data, was computed using exponential functions for the radial temperature [$\tilde{T}(\zeta) = 1300.0055 - 0.0055\exp(12.11\zeta^2)$] and CO partial pressure [$\tilde{P}_{CO}(\zeta) = 4.000011 - 0.000011\exp(12.11\zeta^2)$]. These synthetic profiles represent a mixing region that is 10% of the cross-sectional radius (small purge gas mixing region). Temperature and CO partial pressure were recovered by using seven different spectral ranges, each covering 80 cm^{-1}. The results are shown in Table 1 for the different ranges. The LOS temperature is within 50 K of the centerline value as long as the data-reduction algorithm uses spectral transmittance data below 2030 cm^{-1} [$E' > 0.65E(1300\text{ K})$ for all transmittance data]. This is consistent with Fig. 4, where the mixing region has a minimal impact on the integrated absorption coefficient for $E' > 0.6E(T_c)$ when both temperature and partial pressure decrease within the mixing region ($T_c > T_p$ and $P_{i,c} > P_{i,p}$). The predicted LOS-average temperatures will continually decrease as more spectral transmittance points are used corresponding to rovibrational lines with $E' < E(1300\text{ K})$. In addition, the considered noise levels have little effect on the predicted LOS-average values. The LOS average partial pressures of CO are off by 10% from the true centerline values for almost all of the cases. Hence, LOS-average temperature and partial pressures can be found by using spectral regions in which the mixing region has a minor contribution to the transmittance data.

Large Purge Gas Mixing Region

Synthetic transmittance data were also generated using more extensive radial variations in temperature [$\tilde{T}(\zeta) = 1331.4604 - 31.4604\exp(3.49\zeta^2)$] and CO partial pressure [$\tilde{P}_{CO}(\zeta) = 4.06292 - 0.06292\exp(3.49\zeta^2)$] to demonstrate the ability of the algorithm to deduce flame core parameters when a significant low-temperature gas region is present within the probe volume. These profiles have a 50% reduction in the temperature and partial pressure when $\zeta = 0.9$. The LOS-average temperature is off by 150 K from the centerline value when all data points have transitions with $E' > E(1300\text{ K})$, and it is off by about 300 K when all data points have transitions with $E' < E(1300\text{ K})$. All of the predicted LOS-average CO partial pressures were significantly different from the centerline value of 4 atm.

The approach was also utilized to determine temperature and CO partial-pressure profiles for three different spectral ranges, each covering 80 cm^{-1}. Figure 5 shows a comparison of the temperature and partial-pressure profiles deduced from the three different spectral regions with the input profiles. Within the figure, points represent the input exponential profiles and the lines are the deduced profiles using a sixth-order power series. No significant improvements in temperature and species profiles are seen beyond a sixth-order power series approximation; therefore, all three ranges were run with sixth-order power series approximations for temperature and CO partial pressure. The spectral range that used only rovibrational

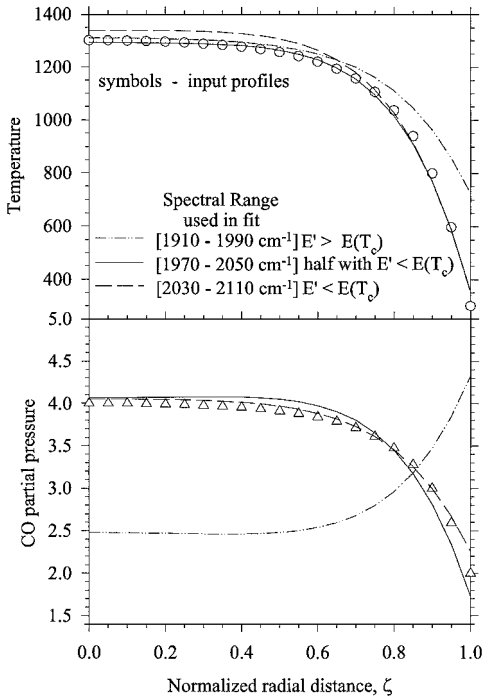

Fig. 5 Influence of spectral range on the ability to deduce temperature and partial-pressure profiles when a significant cool gas region exists within the probe volume.

transitions with $E' > E(T_c)$ could not back out reasonable profiles. The centerline temperature was close to the actual value whereas the centerline partial pressure was significantly different. This spectral range does not have rovibrational transitions that are sensitive to the low-temperature portion of the mixing region, and therefore, cannot reproduce the outer edge of the temperature profile. The other two regions, however, are able to reproduce the temperature and CO partial-pressure profiles. These two regions contain sufficient information on low-temperature transitions to reproduce the radial profiles. Similar results were found when the noise level was as high as 0.005. Species and temperature profiles can be found by using spectral regions that consists of rovibrational transitions that are sensitive to a wide range of temperatures.

Interference of Rovibrational Bands

Working at high temperatures and pressures will increase the extent of interference between molecular rovibrational bands. For instance, the P branch of the fundamental CO band contains H_2O rovibrational lines, wings from the R branch of NO, and excited bands from CO_2. The data-reduction algorithm can easily be extended to solve for concentrations of multiple species simultaneously. The addition of these species will influence the results, especially in the small mixing region case where it may be difficult to find a single spectral range that has transitions with $E' > E(T)$ for all molecules. For instance, only a small spectral region of the R branch of NO is sensitive to high temperatures because this molecule has a narrow vibrational band width. The algorithm was able to deduce accurate temperature and core partial pressures when both CO and NO were included in the synthetic data. However, when the algorithm includes the solution of a baseline fit, the partial pressure of NO is significantly underpredicted. A slightly higher spectral resolution ($1\ cm^{-1}$) will allow the measurement of NO rotational line structure and decouple the baseline from the NO rovibrational band structure. This allows CO and NO partial pressures to be found simultaneously.

At this time, the most troubling aspect of the data-reduction algorithm is the inaccuracy of the HITRAN database at high temperatures. CO_2, NO, and H_2O are all missing rovibrational transitions that are important at temperatures greater than 1000 K. Comparisons of measured and calculated (using the HITRAN database) high-temperature CO_2 and H_2O spectra in Refs. 23 and 24, respectively, demonstrate inadequacies of the HITRAN database. Predicted H_2O absorption coefficients based on the HITRAN database are at least a factor of two smaller than measured data in regions that are sensitive to higher temperatures and by a factor of 1.5 in regions sensitive to lower temperatures, such as the 3750–3950 cm^{-1} range. HITRAN significantly underpredicts the absorption coefficients of both H_2O and CO_2 in the 2000–2150 cm^{-1} range. This will impact the partial-pressure predictions of CO. Investigators have begun to develop high-temperature databases for H_2O (Ref. 24) and CO_2 (Ref. 25); however they contain 300,000–400,000 lines, compared to HITRAN, which has 30,000–40,000 lines. This increase in the number of rovibrational transitions will significantly increase the computational time needed for line-by-line spectral transmittance calculations.

C. Characterization of Noise Within FTIR Spectra

As demonstrated previously,[13] noise affects the deduced temperature and species profiles. With this in mind, it is important to characterize the noise within FTIR spectra. Histograms of noise within the spectrum provide an estimate of the statistical distribution, while the variation in noise level with wavenumber depends inversely on the signal intensity given by[20]

$$F_{\text{noise}}(\nu) = F(\nu) + \omega(\nu)\sigma_s / B_b(\nu) \tag{12}$$

This relationship allows the noise over any wavenumber range to be estimated if the noise can be calculated anywhere within the spectrum. An accurate account of noise allows for an estimate of errors in the deduced temperature and partial pressures by using Eq. (7). The validity of Eq. (12) is seen through Fig. 6, which shows a comparison of the normalized background signal $[I(\nu)/I(\nu = 2500\ cm^{-1})]$ with the inverted normalized noise $[\sigma(\nu = 2500\ cm^{-1})/\sigma(\nu)]$. The normalized noise at 2000 cm^{-1} demonstrates the influence of atmospheric H_2O on the noise within the spectrum. The background water signal leads to a lower intensity, thereby increasing the noise level within the transmittance data.

A histogram of noise within the measured transmittance, taken without a flame, is well represented by a Gaussian distribution function, as shown in Fig. 7. The noise was determined by subtracting a linear fit of the transmittance spectrum from the transmittance spectrum itself over the 2600–2800 cm^{-1} range. Histograms of noise within the spectrum taken from different wavenumber ranges and spectra through flames are also well represented by a Gaussian distribution function.

D. Temperature and Species Measurements in Solid-Propellant Flames

The inverse algorithm is used to determine temperature and species mole fractions from FTIR spectra acquired during the

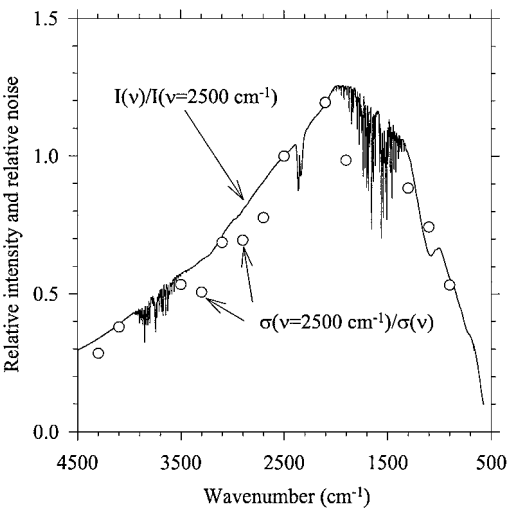

Fig. 6 Variations in noise level and background signal intensity with wavenumber.

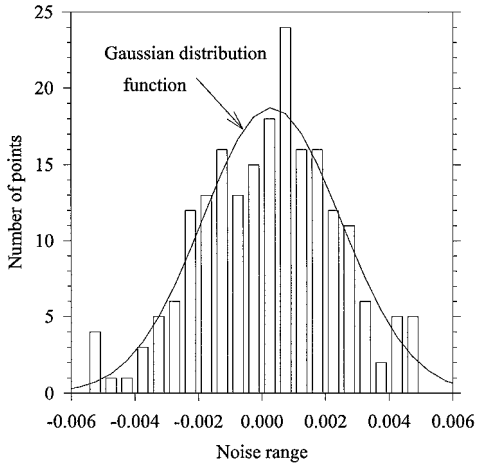

Fig. 7 Histogram of FTIR noise taken from an FTIR transmittance spectrum over the 2600–2800 cm^{-1} range.

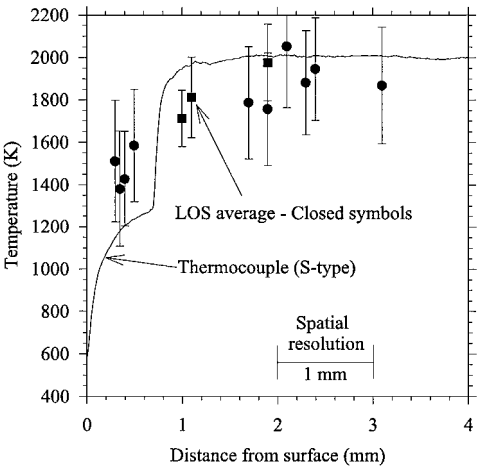

Fig. 9 Temperature profiles of an XM39 propellant flame at 22 atm using FTIR spectroscopy and Pt/Pt-10% Rh (S-type) thermocouple.

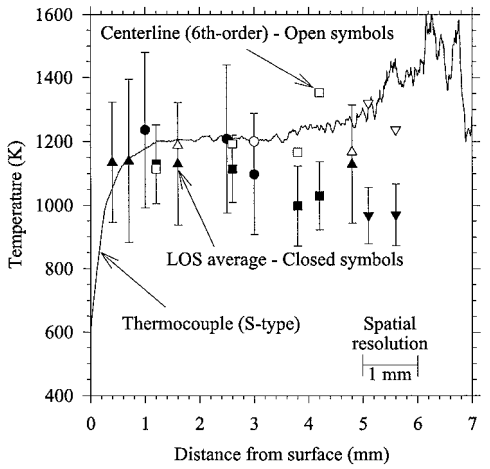

Fig. 8 Temperature profiles of an XM39 propellant flame at 15 atm using FTIR spectroscopy and Pt/Pt-10% Rh (S-type) thermocouple.

steady-state combustion of XM39. The fundamental band of CO is used to determine LOS-average and radial variations in temperature and CO partial pressure. The deduced temperatures are then used to determine the partial pressures of other IR-active species. Temperatures deduced from FTIR spectra are compared to thermocouple measurements.

Temperature Measurements

The temperatures deduced from FTIR spectra are compared to thermocouple measurements (S-type) in Figs. 8 and 9 for steady-state combustion of XM39 at 15 atm and 22 atm, respectively. The closed-faced symbols are LOS-average values, the open-faced symbols are centerline values from sixth-order power series approximation for the radial temperature profiles, and the lines represent thermocouple data. Four FTIR tests at 15 atm and two tests at 22 atm are shown to demonstrate the repeatability. Figure 8 shows that the LOS-average temperatures are within 70 K of the thermocouple traces near the surface (less than 3 mm from the surface) for the 15 atm tests, although the LOS-average values are 200–300 K less than the thermocouple measurements further above the surface. LOS-average and centerline temperatures both match the thermocouple readings near the surface where the mixing region is small. The data-reduction algorithm provided a good fit to the spectra acquired near the surface, as indicated by the value of χ^2 and a visual comparison between the measured and fitted spectra. Further from the surface, the mixing region grows, leading to a significant cool gas region within the probe volume thus causing the LOS-average temperature to be significantly different from thermocouple measurements. In this region of the flame, the use of LOS-average temperatures and partial pressures within the algorithm resulted in poor fits (based on χ^2) to the acquired spectra. However, the centerline values from deduced sixth-order power series profiles reproduce the thermocouple trace. Error bars (95% confidence limits) on the LOS-average values were calculated from Eq. (7). Estimates of the noise within the CO transmittance data, required in Eq. (7), were made using Eq. (12) and measured noise from the 2500–2600 cm^{-1} range. Temperatures and CO partial pressures were determined from CO spectra over the 2000–2090 cm^{-1} range. The lower limit was chosen to minimize interference from NO, whereas the upper limit was chosen to minimize the number of transitions with $E' < E(1200\,\text{K})$.

Tests performed at 22 atm show the presence of a dark zone, varying in length from 0.5 to 2.0 mm. This variation in dark-zone length coupled with a slightly uneven burning surface, with respect to the FTIR beam, leads to vertical variations within the probe volume. The vertical variations are noticeable in FTIR spectra taken near the surface, where high-temperature CO transitions are observed in the low-temperature NO band structure, as well as in recorded images taken during combustion. Only LOS-average values were determined at this pressure. Beyond 2 mm from the surface, LOS-average temperatures are within 100 K of the thermocouple traces. The LOS-average values determined below 2 mm strongly depend on the species and spectral ranges used for data reduction. The 1950–2030 cm^{-1} range was used to determine temperatures and CO partial pressures above 2 mm. Interference from NO is small at high temperatures allowing a spectral region that is more sensitive to high-temperature CO transitions to be used. Temperatures obtained from thermocouples and spectral transmittances are slightly lower than the adiabatic flame temperature of 2163 K for XM39 at 22 atm (Ref. 26); radiative heat losses and incomplete combustion are believed to contribute to this discrepancy.

Species Measurements

Figure 10 shows the deduced CO and NO mole-fraction profiles of the XM39 flame at 15 atm. Within this figure, the closed-faced symbols are LOS-averaged values whereas the open-faced symbols are centerline values from sixth-order power series approximations for the radial profiles. CO mole fractions and temperatures were deduced from the FTIR spectra using the 2000–2090 cm^{-1} range, whereas NO mole fractions were determined using the 1880–1950 cm^{-1} range. The narrow vibrational band width and lack of radiative properties beyond 1950 cm^{-1} for NO dictated the use of this spectral range that is sensitive to high and low temperature rovibrational transitions. Close to the surface (3 mm <), no significant corrections for spatial variations in CO mole fractions were determined from the spectral transmittance measurements, and therefore, only LOS-average values are shown in this region in Fig. 10. Beyond 3 mm, spatial variations in NO and CO mole fractions were found

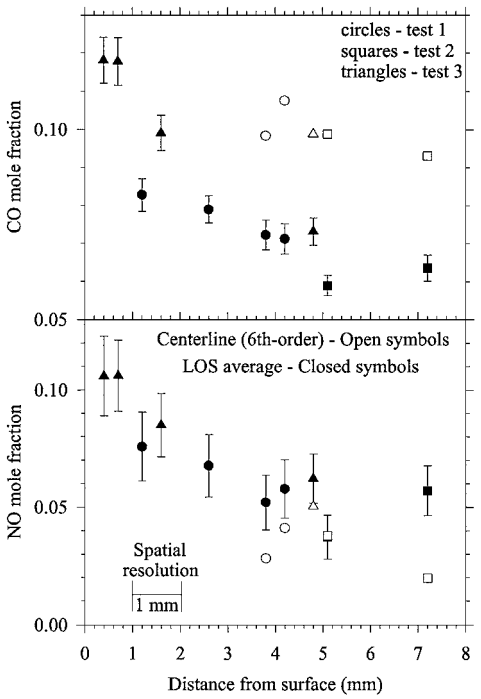

Fig. 10 Deduced CO and NO mole-fraction profiles of an XM39 flame at 15 atm.

from spectral transmittance measurements using the data-reduction algorithm. Corrected CO mole fractions (centerline values of sixth-order power series) were larger than predicted LOS-average values, whereas corrected NO mole fractions are slightly less than LOS-average values. The algorithm is able to use the spectral variations in transmittances to correct for spatial variations in CO and NO. Within Fig. 10, 95% confidence limits on the LOS values were calculated using Eq. (7).

The FTIR flame spectra also indicated the presence of CO_2, N_2O, H_2O, HCN, and CH_4. LOS-average mole fractions of these species were found close to the surface. Further from the surface, the algorithm was not able to determine radial profiles for these molecules. The determination of spatial variations for these molecules should be possible when accurate high-temperature radiative properties are known.

IV. Future Work

To increase the confidence and applicability of the developed technique, work in two areas are suggested. First and most important is the lack of accurate radiative property data of many IR-active molecules at high temperatures, including line strength, transition frequencies, and the dependence of the pressure broadened half-width on temperature, pressure, and the partial pressures of other combustion products. Second, more accurate flame diameters should be measured and different approximations for the radial variations in temperature and partial pressures should be assessed. In addition, accurate models of line-mixing and sub-Lorentzian behavior of rovibrational lines are also needed to determine spatial variations in temperature and species partial pressure from spectral transmittances accurately.

V. Conclusions

This work described the development and use of an inverse algorithm for deducing temperature and species profiles within solid-propellant flames by employing spectral transmittance data acquired by an FTIR spectrometer. Mass spectroscopy was used to validate the inverse algorithm. The major findings are as follows.

1) FTIR and MPMS measurements of relative mole-fraction profiles of CO, CO_2, NO, N_2O, and NO_2 taken during laser-assisted deflagration of XM39 at 1 atm and 65 W/cm^2 agreed in both magnitude and trend.

2) LOS-average temperature and partial pressures were found from transmittance data when a small purge gas mixing region exists at the edge of the flame. The use of rovibrational transitions with high lower-state energies minimizes the impact of the cool mixing region on the LOS measurements.

3) Radial temperature and partial-pressure profiles were determined from transmittance data when a large cool-gas mixing region exists at the periphery of the flame. The use of spectral regions for data reduction that are sensitive to high and low temperature transitions allows an accurate determination of flame temperature and partial pressures.

4) Temperatures deduced from FTIR spectra acquired during steady-state combustion of XM39 at 15 and 22 atm matched data acquired by thermocouples. Near the surface, only a thin mixing region exists allowing the deduced LOS-average temperatures to be in good agreement with data obtained from thermocouples. Further up in the flame, LOS-average temperatures were 200–300 K lower than thermocouple data because of a large cool-gas mixing region. Centerline values deduced from a sixth-order power series for radial temperature profiles were able to reproduce the thermocouple-based data further up in the flame.

5) Measured spectral transmittances from the XM39 flame were used to determine LOS average and radial variations in the mole fractions of CO and NO. LOS-average values were deduced close to the surface, whereas centerline values from the deduced radial variations were used to give NO and CO mole fractions further into the flame.

6) Radial variations in the mole fractions of CO_2, H_2O, HCN, N_2O, and CH_4 could not be determined using the data-reduction algorithm because of inaccuracies in the high-temperature radiative properties of these molecules.

Acknowledgments

This work was performed at Pennsylvania State University under Contract DAAL03-92-G-0118 and supported by R. W. Shaw of the U.S. Army Research Office, Research Triangle Park, NC.

References

[1]Liau, Y. C., and Yang, V., "Analysis of RDX Monopropellant Combustion with Two-Phase Subsurface Reactions," *Journal of Propulsion and Power*, Vol. 11, No. 4, 1995, pp. 729–739.

[2]Prasad, K., Yetter, R. A., and Smooke, M., "An Eigenvalue Method for Computing the Burning Rates of HMX Propellants," *Combustion and Flame*, Vol. 115, No. 3, 1998, pp. 406–416.

[3]Melius, C. F., "Thermochemical Modeling: I & II," *Chemistry and Physics of Energetic Materials*, edited by S. N. Bulusu, Kluver Academic, Norwell, MA, 1990, pp. 21–78.

[4]Yetter, R. A., Dryer, F. L., Allen, T., and Gatto, J., "Analysis of Elementary Models for the Steady-State Combustion of Solid Propellants," *Journal of Propulsion and Power*, Vol. 11, No. 4, 1995, pp. 666–676.

[5]Parr, T., and Hanson-Parr, D., "Nonintrusive Diagnostic Technique for Research on Nonsteady Burning of Solid Propellants," *Nonsteady Burning and Combustion Stability of Solid Propellants*, edited by L. De Luca, E. W. Price, and M. Summerfield, Vol. 143, Progress in Astronautics and Aeronautics Series, AIAA, Washington, DC, 1992, Chap. 8.

[6]Vanderhoff, J. A., "Species Profiles in Solid Propellant Flames Using Absorption and Emission Spectroscopy," *Combustion and Flame*, Vol. 84, No. 1–2, 1991, pp. 73–92.

[7]Lu, Y. C., Freyman, T. M., and Kuo, K. K., "Measurement of Temperatures and OH Concentrations of Solid Propellant Flames Using Absorption Spectroscopy," *Combustion Science and Technology*, Vol. 104, Nos. 1–3, 1995, pp. 193–205.

[8]Modiano, S. H., and Vanderhoff, J. A., "Multichannel Infrared Absorption Spectroscopy of Solid Propellant Flames," *Combustion and Flame*, Vol. 99, No. 1, 1994, pp. 187–189.

[9]Mallery, C. F., and Thynell, S. T., "Species and Temperature Profiling of Propellant Flames Using FTIR Absorption Spectroscopy," *Combustion Science and Technology*, Vol. 122, No. 1–6, 1997, pp. 113–129.

[10]Cremers, C. J., "Application of Abel's Integral Equation to Spectroscopic Data," *Applied Optics*, Vol. 5, No. 6, 1966, pp. 1057–1064.

[11]McNesby, K. L., Daniel, R. G., Morris, J. B., and Miziolek, A. W., "Tomographic Analysis of CO Absorption in a Low-Pressure Flame," *Applied Optics*, Vol. 34, No. 18, 1995, pp. 3318–3324.

[12]Best, P. E., Chien, P. L., Carangelo, R. M., Solomon, P. R., Danchak, M., and Llovici, I., "Tomographic Reconstruction of FT-IR Emission and

Transmission Spectra in a Sooting Laminar Diffusion Flame: Species Concentrations and Temperatures," *Combustion and Flame*, Vol. 85, No. 3–4, 1991, pp. 309–318.

[13]Mallery, C. F., and Thynell, S. T., "Line-of-Sight Temperature and Species Profiles Determined from Spectral Transmittances," *Journal of Thermophysics and Heat Transfer*, Vol. 11, No. 3, 1997, pp. 367–374.

[14]Griffiths, P. R., and de Haseth, J. A., *Fourier Transform Infrared Spectrometry*, Wiley, New York, 1986.

[15]Rothman, L. S., Gamache, R. R., Tipping, R. H., Rinsland, C. P., Smith, M. A. H., Benner, C., Devi, M. V., Flaud, J.-M., Camy-Peyret, C., Perrin, A., Goldman, A., Massie, S. T., Brown, L., and Toth, R. A., "The HITRAN Molecular Database: Editions of 1991 and 1992," *Journal of Quantitative Spectroscopy and Radiative Transfer*, Vol. 48, Nos. 5/6, 1992, pp. 469–507.

[16]Press, W. H., Teukolsky, S. A., Vetterling, W. T., and Flannery, B. P., *Numerical Recipes*, Cambridge Univ. Press, Cambridge, MA, 1992.

[17]Özisik, M. N., "Inverse Heat Conduction Problems (IHCP)," *Heat Conduction*, 2nd ed., Wiley, New York, 1993, Chap. 14.

[18]Ho, C.-H., and Özisik, M. N., "An Inverse Radiation Problem," *International Journal of Heat and Mass Transfer*, Vol. 32, No. 2, 1989, pp. 335–341.

[19]Litzinger, T., Fetherolf, B., Y. Lee, Y.-J., and Tang, C. J., "Study of the Gas-Phase Chemistry of RDX: Experiments and Modeling," *Journal of Propulsion and Power*, Vol. 11, No. 4, 1995, pp. 698–703.

[20]Mallery, C. F., Jr., "Radial Temperature and Species Profiles from an Inverse Analysis of Spectral Transmittances," Ph.D. Thesis, Dept. of Mechanical Engineering, Pennsylvania State Univ., University Park, PA, Aug. 1997.

[21]Mallery, C. F., and Thynell, S. T., "Line-of-Sight Profiling of Temperature and Species in Propellant Flames Using FTIR Spectroscopy," AIAA Paper 98-3827, July 1998.

[22]Ouyang, X., and Varghese, P. L., "Line-of-Sight Absorption Measurements of High Temperature Gases with Thermal and Concentration Boundary Layer," *Applied Optics*, Vol. 28, No. 18, 1989, pp. 3979–3984.

[23]Scutaru, D., Rosenmann, L., Taine, J., Wattson, R. B., and Rothman, L. S., "Measurements and Calculations of CO_2 Absorption at High Temperature in the 4.3 and 2.7 μm Regions," *Journal of Quantitative Spectroscopy and Radiative Transfer*, Vol. 50, No. 2, 1993, pp. 179–191.

[24]Rivière, Ph., Langlois, S., Soufiani, A., and Taine, J., "An Approximate Data Base of H_2O Infrared Lines for High Temperature Applications at Low Resolution. Statistical Narrow-Band Model Parameters," *Journal of Quantitative Spectroscopy and Radiative Transfer*, Vol. 53, No. 2, 1995, pp. 221–234.

[25]Scutaru, D., Rosenmann, L., and Taine, J., "Approximate Intensities of CO_2 Hot Bands 2.7, 4.3, and 12 μm for High Temperature and Medium Resolution Applications," *Journal of Quantitative Spectroscopy and Radiative Transfer*, Vol. 52, No. 6, 1994, pp. 765–781.

[26]Gordon, S., McBride, B. J., and Zeleznic, F. J., "Computer Program for Calculation of Complex Chemical Equilibrium Composition and Applications, Suppl. I, Transport Properties," NASA, Washington, DC, 1984.